A New Trajectory Branching Approximation To Propagate the Mixed Quantum–Classical Liouville Equation

ARTICLE *in* THE JOURNAL OF PHYSICAL CHEMISTRY A · JUNE 2014

Impact Factor: 2.69 · DOI: 10.1021/jp503522g · Source: PubMed

3 AUTHORS:

Shuming Bai

Aix-Marseille Université

12 PUBLICATIONS **47** CITATIONS

SEE PROFILE

Xww Xww

Chinese Academy of Sciences

5 PUBLICATIONS **26** CITATIONS

SEE PROFILE

Qiang Shi

Chinese Academy of Sciences

101 PUBLICATIONS **2,414** CITATIONS

SEE PROFILE

THE JOURNAL OF PHYSICAL CHEMISTRY A

Article

pubs.acs.org/JPCA

A New Trajectory Branching Approximation To Propagate the Mixed Quantum-Classical Liouville Equation

Shuming Bai, Weiwei Xie, and Qiang Shi*

Beijing National Laboratory for Molecular Sciences, State Key Laboratory for Structural Chemistry of Unstable and Stable Species, Institute of Chemistry, Chinese Academy of Sciences, Zhongguancun, Beijing 100190, China

ABSTRACT: Starting from the mixed quantum-classical Liouville (MQCL) equation, we derive a new trajectory branching method as a modification to the conventional mean field approximation. In the new method, the mean field approximation is used to propagate the mixed quantum-classical dynamics for short times. When the mean field description becomes invalid, new trajectories are added in the simulation by branching the single trajectory into multiple ones. To achieve this, a new set of variables are defined to monitor the deviations of the dynamics on different potential energy surfaces from the reference mean field trajectory, and their equations of motion are derived from the MQCL equation based on the method of first moment expansion. The new method is tested on several one-dimensional two surface problems and is shown to correctly solve the problem of the mean field approximation in several cases.

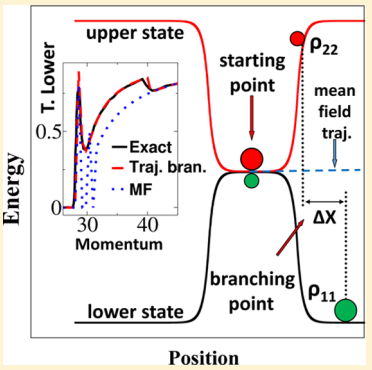

1. INTRODUCTION

The microscopic world of molecules is governed by the law of quantum mechanics. Yet due to the unfavorable scaling of the computational costs with the number of degrees of freedom (DOFs) in solving the Schrödinger equation, accurate simulation of quantum dynamics in the condensed phase still presents a significant challenge in theoretical chemistry.[1] Over the past years, numerically exact methods with much improved efficiency have been developed, such as the multiconfiguration time-dependent Hartree (MCTDH),[2−4] path integral,[5,6] and hierarchical equations of motion (HEOM) methods.[7−9] However, these methods can only handle systems with limited size and are often restricted to specific forms of model Hamiltonians.

Other approximate methods that are able to deal with large systems are also developed, such as the semiclassical methods.[10−14] Various types of mixed quantum-classical methods are also proposed,[15−20] where the light particles are treated quantum mechanically, and the heavy particles are treated classically. In literature, many problems can be subject to such mixed quantum-classical treatments, including molecular scattering,[17] electron and proton transfer in the condensed phase,[21−23] nonadiabatic dynamics in photochemistry,[24] linear and nonlinear spectroscopy,[25,26] and molecular dynamics under strong laser pulses.[27,28]

When the Born−Oppenheimer (BO) approximation[29] is valid, the mixed quantum-classical treatment reduces to classical dynamics on a single potential energy surface and can readily be applied to simulations of large systems. However, when the BO approximation breaks and dynamics on different potential energy surfaces are coupled, solving the resulted nonadiabatic dynamics is not a trivial task. The most commonly used mixed quantum-classical methods include the mean field[15,16,30,31] and surface hopping (SH)[17,18,32−34] methods. The mean field method assumes that dynamics of the classical DOFs is governed by the "average forces" determined by the wave function of the quantum DOFs. Although the mean field method can often correctly capture the short time dynamics,[23,24] it is known that the long time dynamics has many problems including violations of detailed balance.[24,35−37] The average force approximation may also lead to unphysical results for dynamics involving very different potential energy surfaces.[38]

In the SH method, the classical DOFs evolve on predefined potential energy surfaces and hop between different potential energy surfaces stochastically, which is affected by the dynamics of the quantum DOFs. The fewest-switches surface-hopping (FSSH) developed by Tully[17] is the most popular algorithm and has been widely used in simulating multidimensional nonadiabatic dynamics. The feature that the classical DOFs evolve on different realistic potential energy surfaces contributes to the wide success of the SH method, which avoids the deficiency of averaged forces used in the mean field method.

Although the classical DOFs hop stochastically between different potential energies, and a number of trajectories are averaged to get the final results, the SH method also employs a single trajectory description of the mixed quantum-classical dynamics. As such, both the mean field and SH methods are known to have the problem of "overcoherence" which originates from the fact that the quantum wave function is

Special Issue: International Conference on Theoretical and High Performance Computational Chemistry Symposium

Received: April 10, 2014
Revised: June 9, 2014

   dx.doi.org/10.1021/jp503522g | J. Phys. Chem. A XXXX, XXX, XXX−XXX

propagated coherently along a single classical trajectory for all times.[18,39−41] A general procedure to solve the problem of decoherence is to collapse the coherent wave function onto a "pure" state stochastically by a certain algorithm.[18,39−43] The idea of trajectory branching has also been proposed to go beyond the single trajectory description, by adding new trajectories during the time-dependent evolution.[44−46] For example, in the method proposed by Takatsuka and co-workers, the trajectory in phase space will branch into multiple ones for their own individual eigenforces when nonadiabatic coupling becomes sufficiently small.[44]

In recent years, there are also intensive interests in the mixed quantum-classical Liouville (MQCL) equation, which can be obtained by taking the proper classical limit of the partial Wigner transformed quantum mechanical Liouville equation,[19,47−49] or the path integral methods.[50] The MQCL equation is based on a more rigorous approximation, whereas it is currently very difficult to propagate the MQCL for long time dynamics, despite some recent advances in the numerical algorithms.[51−54] Although some recent studies combining the MQCL (or the partial linearized path integral) approach and the mapping Hamiltonian method[11,15] may provide a promising way to simulate mixed quantum-classical dynamics,[55−58] development of new and efficient methods to solve the MQCL equation is still an active topic in the area of nonadiabatic dynamics.

The density matrix form of the MQCL equation also offers more flexibility over the mean field and SH methods. It has been shown that the later two methods can be derived from the MQCL method with additional approximations.[47,49,59−61] The MQCL equation can also be used to improve both the mean field and SH methods. For example, Subotnik and co-workers have used the MQCL equation to derive a new parameter free dephasing rate for the surface-hopping dynamics.[42] In a recent work, we have also derived a modified mean field method to calculate absorption spectra involving multiple excited states.[62]

In this work, we propose a new trajectory branching approximation for the MQCL equation of motion. Starting from the MQCL equation, we first obtain the mean field dynamics of the classical DOFs for a single trajectory, and define two auxiliary variables that are used to monitor the validity of the single trajectory approximation. Equations of motion for the auxiliary variables are obtained by first-order moment expansion near the mean field reference trajectory. We then present the new trajectory branching algorithm based on a novel branching criterion. The new method is then tested with a series of one-dimensional two state models from previous studies.[17,42]

The remaining parts of the article are organized as follows. In section 2, we present the mixed quantum-classical Liouville equation in the adiabatic basis set, derivation of the equations of motion for the auxiliary variables, and details of the new trajectory branching algorithm. In section 3, we apply the new method to several one-dimensional two surface models and compare the results with the quantum and mean field ones. Finally, conclusions and discussions are made in section 4.

2. THEORY

Consider the following total Hamiltonian that describes a quantum subsystem coupled to a group of heavy particles that are to be treated classically,

$$\hat{H} = \hat{H}_S(\hat{p},\hat{q}) + \hat{H}_B(\hat{\mathbf{P}},\hat{\mathbf{Q}}) + \hat{V}_{SB}(\hat{q},\hat{\mathbf{Q}}) \tag{1a}$$

$$\hat{H}_S(\hat{p},\hat{q}) = \frac{\hat{p}^2}{2\mu} + \hat{V}_S(\hat{q}) \tag{1b}$$

$$\hat{H}_B(\hat{\mathbf{P}},\hat{\mathbf{Q}}) = \sum_j \frac{\hat{P}_j^2}{2M_j} + \hat{V}_B(\hat{\mathbf{Q}}) \tag{1c}$$

where $\hat{p}$, $\hat{q}$ are the momentum and coordinate of the quantum subsystem, $\hat{\mathbf{P}}$, $\hat{\mathbf{Q}}$ are those of the heavy particles. $\hat{H}_S$ and $\hat{H}_B$ are Hamiltonians of the quantum system and classical bath, and $\hat{V}_{SB}$ describes the coupling between them. For simplicity, we consider only one degree of freedom for the quantum subsystem, and further assume that all the heavy particles have the same mass, $M_j = M$.

We now briefly sketch the derivation of the MQCL equation based on the method of partial Wigner transformation.[19,49,54] The quantum Liouville equation for the total density operator $\hat{\rho}_T$ is given by

$$\frac{\partial\hat{\rho}_T}{\partial t} = -\frac{i}{\hbar}[\hat{H},\hat{\rho}_T] \tag{2}$$

and the partial Wigner transform[63] of ρ_T is defined as

$$\rho_w(\mathbf{Q},\mathbf{P}) = \frac{1}{(2\pi\hbar)^N}\int d\Delta\, e^{-(i/\hbar)\mathbf{P}^T\cdot\Delta}\langle\mathbf{Q}+\Delta/2|\hat{\rho}_T|\mathbf{Q}-\Delta/2\rangle \tag{3}$$

After doing the partial Wigner transform of the quantum Liouville equation in eq 2, and taking the classical limit $\hbar \to 0$, the MQCL is given by[19,49,64]

$$\frac{\partial\rho_w}{\partial t} = -\frac{i}{\hbar}[\hat{H}_w,\rho_w] + \frac{1}{2}[\{\hat{H}_w,\rho_w\} - \{\rho_w,\hat{H}_w\}] \tag{4}$$

where H_w is the partial Wigner transform of the total Hamiltonian $\hat{H}$.

The above eq 4 is in an operator form for the quantum subsystem, and a basis set is needed in realistic calculations. The adiabatic basis set is adopted in this work, where the basis set ϕ_j is defined as the eigenstate of the Hamiltonian $\hat{H}_S + \hat{V}_{SB}$:

$$[\hat{H}_S(\hat{p},\hat{q}) + \hat{V}_{SB}(\hat{q},\mathbf{Q})]|\phi_j\rangle = E_j(\mathbf{Q})|\phi_j\rangle \tag{5}$$

In the literature, there are two slightly different forms of the MQCL equation in the adiabatic basis set, depending on the order of partial Wigner transform and the expansion into the adiabatic basis set. In the first form adopted by Kapral and co-workers,[19] the partial Wigner transform is done before the basis set expansion, and the resulting equation of motion is given by (for simplicity, we have dropped the subscript "w" for the partial Wigner transform in following derivations)

$$\begin{aligned}\frac{\partial}{\partial t}\rho_{ij}(\mathbf{P},\mathbf{Q};t) &= -\frac{i}{\hbar}[E_i(\mathbf{Q}) - E_j(\mathbf{Q})]\rho_{ij}(\mathbf{P},\mathbf{Q};t)\\ &- \left[\frac{\mathbf{P}}{M}\cdot\nabla_{\mathbf{Q}} + \frac{\mathbf{F}_i(\mathbf{Q}) + \mathbf{F}_j(\mathbf{Q})}{2}\cdot\nabla_{\mathbf{P}}\right]\rho_{ij}(\mathbf{P},\mathbf{Q};t)\\ &- \sum_k\left(\frac{\mathbf{P}}{M}\cdot\mathbf{d}_{ik}(\mathbf{Q}) + \frac{1}{2}\mathbf{F}_{ik}(\mathbf{Q})\cdot\nabla_{\mathbf{P}}\right)\rho_{kj}(\mathbf{P},\mathbf{Q};t)\\ &- \sum_k\left(-\frac{\mathbf{P}}{M}\cdot\mathbf{d}_{kj}(\mathbf{Q}) + \frac{1}{2}\mathbf{F}_{kj}(\mathbf{Q})\cdot\nabla_{\mathbf{P}}\right)\rho_{ik}(\mathbf{P},\mathbf{Q};t)\end{aligned} \tag{6}$$

where $\mathbf{d}_{ij}(\mathbf{Q}) = \langle\phi_i(\mathbf{Q})|\nabla_{\mathbf{Q}}|\phi_j(\mathbf{Q})\rangle$ is the nonadiabatic coupling vector, and $\mathbf{F}_{ij} = -\langle\phi_i(\mathbf{Q})|\partial(\hat{V}_{SB} + V_B)/\partial\mathbf{Q}|\phi_j(\mathbf{Q})\rangle$ is the force

dx.doi.org/10.1021/jp503522g | J. Phys. Chem. A XXXX, XXX, XXX−XXX

term. Using the Hellmann−Feynman theorem, the diagonal terms can be written as to $\mathbf{F}_j \equiv \mathbf{F}_{jj} = -\partial(E_j + V_B)/\partial\mathbf{Q}$, the off-diagonal terms are $\mathbf{F}_{ik} = [E_i(\mathbf{Q}) - E_k(\mathbf{Q})]\mathbf{d}_{ik}(\mathbf{Q})$.

In another form adopted by Ando and co-workers,[49] the basis set expansion proceeds the partial Wigner transform, and the equation of motion is given by

$$\frac{\partial}{\partial t}\rho_{ij}(\mathbf{P},\mathbf{Q};t) = -\frac{\mathrm{i}}{\hbar}[E_i(\mathbf{Q}) - E_j(\mathbf{Q})]\rho_{ij}(\mathbf{P},\mathbf{Q};t) - \left[\frac{\mathbf{P}}{M}\cdot\nabla_{\mathbf{Q}} + \frac{\mathbf{F}_i(\mathbf{Q}) + \mathbf{F}_j(\mathbf{Q})}{2}\cdot\nabla_{\mathbf{P}}\right]\rho_{ij}(\mathbf{P},\mathbf{Q};t) - \sum_k \frac{\mathbf{P}}{M}\cdot\mathbf{d}_{ik}(\mathbf{Q})\,\rho_{kj}(\mathbf{P},\mathbf{Q};t) + \sum_k \frac{\mathbf{P}}{M}\cdot\mathbf{d}_{kj}(\mathbf{Q})\,\rho_{ik}(\mathbf{P},\mathbf{Q};t) \tag{7}$$

In both eqs 6 and 7, the first term gives phase factors for the off-diagonal terms of the density matrix, the second term indicates that the phase space distribution $\rho_{ij}(\mathbf{Q},\mathbf{P})$ evolves on the average of the ith and jth adiabatic potential energy surfaces, and the third and four terms take into account the nonadiabatic coupling between dynamics on different potential energy surfaces. The major difference between eqs 6 and 7 is the so-called off-diagonal force terms [the $^1/_2\mathbf{F}_{ik}(\mathbf{Q})\cdot\nabla_{\mathbf{P}}$ and $^1/_2\mathbf{F}_{kj}(\mathbf{Q})\cdot\nabla_{\mathbf{P}}$ terms].

Equations 6 and 7 should be considered in the same order of approximation, and previous work has shown that they give very similar numerical results in many problems.[49] Although we note that a recent work shows that in cases of conical intersections, eq 6 performs better than eq 7,[65] because the latter needs to calculate a partial Winger transformation of a double valued function, which is not well-defined. We will also see later in section 2.1 that eqs 6 and 7 give slightly different average forces when the mean field approximation is applied. Equation 6 is used in further derivations, although the two different forms of MQCL equation are found to give very similar results in this study.

The MQCL equations in eqs 6 and 7 describe the mixed quantum-classical dynamics using a set of multidimensional phase space distributions, which become very difficult to solve when the number of DOFs becomes large. Many authors have considered trajectory representations based on surface hopping like methods.[50,53,66] But unlike the traditional surface hopping methods, these hopping algorithms use the absolute values of both the diagonal and off-diagonal elements of the density matrix to determine the probabilities in the stochastic hopping. As the result, the trajectories carry less and less weight in long time simulations, which causes convergence problems.

In this work, we propose to use a new trajectory branching method to solve the MQCL equations. The idea of the new method is that dynamics based on the mean field approximation can be used for short times. When the mean field approximation breaks down, which means that the single trajectory approximation is no longer valid, we use a trajectory branching algorithm to represent the dynamics with multiple trajectories. In the following derivations, we start with the mean field approximation, and derive the first-order moment expansion near the mean field approximation, which is used to define the criterion that marks the breakdown of the mean field approximation.

2.1. Mean Field Approximation and First-Order Moment Expansion. Although derivations of the mean field approximation from the MQCL equation are now well-known,[47,59,60] we give a brief outline of the mean field approximation to facilitate the derivations of the first-order moment expansion. To this end, the averages of $\mathbf{P}$ and $\mathbf{Q}$ with regards to the diagonal and off-diagonal phase space distributions are first defined as

$$\tilde{\mathbf{Q}}_{ij} = \int \mathrm{d}\mathbf{Q}\,\mathrm{d}\mathbf{P}\rho_{ij}(\mathbf{Q},\mathbf{P})\mathbf{Q} \tag{8}$$

$$\tilde{\mathbf{P}}_{ij} = \int \mathrm{d}\mathbf{Q}\,\mathrm{d}\mathbf{P}\rho_{ij}(\mathbf{Q},\mathbf{P})\mathbf{P} \tag{9}$$

The expectation values for $\mathbf{Q}$ and $\mathbf{P}$ can be calculated by taking the trace over the quantum DOF,

$$\bar{\mathbf{Q}} = \int \mathrm{d}\mathbf{Q}\,\mathrm{d}\mathbf{P}\sum_j \rho_{jj}(\mathbf{Q},\mathbf{P})\mathbf{Q} = \sum_j \tilde{\mathbf{Q}}_{jj} \tag{10}$$

$$\bar{\mathbf{P}} = \int \mathrm{d}\mathbf{Q}\,\mathrm{d}\mathbf{P}\sum_j \rho_{jj}(\mathbf{Q},\mathbf{P})\mathbf{P} = \sum_j \tilde{\mathbf{P}}_{jj} \tag{11}$$

By using a simple ansantz

$$\rho_{ij}(\mathbf{Q},\mathbf{P}) = \bar{\rho}_{ij}(t)\,\delta(\mathbf{Q}-\bar{\mathbf{Q}}(t),\mathbf{P}-\bar{\mathbf{P}}(t)) \tag{12}$$

we can obtain from eq 6 that

$$\frac{\mathrm{d}}{\mathrm{d}t}\bar{\rho}_{ij} = -\frac{\mathrm{i}}{\hbar}[E_i(\bar{\mathbf{Q}}) - E_j(\bar{\mathbf{Q}})]\bar{\rho}_{ij} - \sum_k \frac{\bar{\mathbf{P}}}{M}\cdot[\mathbf{d}_{ik}(\bar{\mathbf{Q}})\bar{\rho}_{kj} - \mathbf{d}_{kj}(\bar{\mathbf{Q}})\rho_{ik}] \tag{13}$$

The equations of motion for $\bar{\mathbf{Q}}$ and $\bar{\mathbf{P}}$ can be obtained by taking the trace of $\tilde{\mathbf{Q}}_{ij}$ and $\tilde{\mathbf{P}}_{jj}$. It is easy to derive the following equations of motion:[47]

$$\frac{\mathrm{d}}{\mathrm{d}t}\bar{\mathbf{Q}} = \frac{\bar{\mathbf{P}}}{M} \tag{14}$$

$$\frac{\mathrm{d}}{\mathrm{d}t}\bar{\mathbf{P}} = \mathbf{F}_{\mathrm{mf}} = \sum_i\sum_j \mathrm{Re}(\bar{\rho}_{ij})\,\mathbf{F}_{ij}(\bar{\mathbf{Q}}) \tag{15}$$

which give the traditional mean field (Ehrenfest) approximation. We also know from the above equations that both $\bar{\mathbf{Q}}$ and $\bar{\mathbf{P}}$ are real.

We note that, if starting from eq 7 instead of eq 6, a slightly different mean field force will be obtained,

$$\frac{\mathrm{d}}{\mathrm{d}t}\bar{\mathbf{P}} = \mathbf{F}_{\mathrm{mf}} = \sum_j \bar{\rho}_{jj}\mathbf{F}_j(\bar{\mathbf{Q}}) \tag{16}$$

which can be thought as an approximation to the correct mean field force in eq 15.

Shortcomings of the mean field dynamics in eqs 13−15 have been widely investigated before.[24,62] In the MQCL framework, classical trajectories for ρ_{ij} should propagate under different forces on the "potential energy surface" defined by $[(E_i(\mathbf{Q}) + E_j(\mathbf{Q}))/2] + V_B(\mathbf{Q})$. So even if the initial positions and momenta are the same on different surfaces, the classical trajectories soon become different as they evolve under the influence of different forces. This explains why the mean field approximation based on the single trajectory anasatz in eq 12 works only at short times.

Before presenting the new trajectory branching algorithm, we first define the following variables that describe the deviation from the mean field trajectory,

dx.doi.org/10.1021/jp503522g | J. Phys. Chem. A XXXX, XXX, XXX−XXX

$$\mathbf{X}_{ij} = \tilde{\mathbf{Q}}_{ij} - \bar{\mathbf{Q}}\bar{\rho}_{ij} \tag{17}$$

$$\mathbf{\Pi}_{ij} = \tilde{\mathbf{P}}_{ij} - \bar{\mathbf{P}}\bar{\rho}_{ij} \tag{18}$$

We note that under the mean field ansantz in eq 12, both $\mathbf{X}$ and $\mathbf{\Pi}$ are zero.

The next step is to derive the equation of motion for $\mathbf{X}$ and $\mathbf{\Pi}$ using the mean field trajectory as a reference, starting from the MQCL equation in eq 6. This can be done using a similar technique as presented in our previous work,[62] i.e., by expanding the physical variable near the reference trajectory and doing the phase space integrals. The final equations of motion for $\mathbf{X}_{ij}$ and $\mathbf{\Pi}_{ij}$ can be obtained as follows:

$$\frac{\mathrm{d}}{\mathrm{d}t}\mathbf{X}_{ij} = \frac{\mathbf{\Pi}_{ij}}{M} - \frac{\mathrm{i}}{\hbar}[E_i(\bar{\mathbf{Q}}) - E_j(\bar{\mathbf{Q}})]\mathbf{X}_{ij} - \sum_k \frac{\bar{\mathbf{P}}}{M}\cdot[\mathbf{d}_{ik}(\bar{\mathbf{Q}})\mathbf{X}_{kj} - \mathbf{d}_{kj}(\bar{\mathbf{Q}})\mathbf{X}_{ik}] \tag{19}$$

$$\frac{\mathrm{d}}{\mathrm{d}t}\mathbf{\Pi}_{ij} = -\bar{\rho}_{ij}\mathbf{F}_{\mathrm{mf}} + \frac{1}{2}\sum_k (\bar{\rho}_{ik}\mathbf{F}_{kj} + \bar{\rho}_{kj}\mathbf{F}_{ik}) - \frac{\mathrm{i}}{\hbar}[E_i(\bar{\mathbf{Q}}) - E_j(\bar{\mathbf{Q}})]\mathbf{\Pi}_{ij} - \sum_k \frac{\bar{\mathbf{P}}}{M}\cdot[\mathbf{d}_{ik}(\bar{\mathbf{Q}})\mathbf{\Pi}_{kj} - \mathbf{d}_{kj}(\bar{\mathbf{Q}})\mathbf{\Pi}_{ik}] \tag{20}$$

In this work, we did not try to modify the equation of motion for the $\bar{\rho}_{ij}$ and $\bar{\mathbf{Q}}$, $\bar{\mathbf{P}}$ terms as in ref 62. This is due to two reasons: (1) The modified mean field equations, as in ref 62 and previous studies by Horsfield and co-workers,[67,68] still use a single trajectory description, whereas the goal of this work is to go beyond the single trajectory description of the mean field approach using the branching method, in which the traditional mean field approximation should also work for short times. (2) The modified mean field approximations based on moment expansion may have stability issues in certain cases, as found in previous studies.[69] The current treatment is thus similar to Subotnik's work in ref 42, where the first-order correction terms are only used to calculate the dephasing rates, and not to modify original SH dynamics.

2.2. New Trajectory Branching Algorithm. In this work, eqs 19 and 20 are used to calculate the quantities $\mathbf{X}$ and $\mathbf{\Pi}$, which are then used to quantitatively monitor the deviations from the mean field trajectory. If the mean field approach has errors beyond a threshold, we use a trajectory branching algorithm to propagate different elements of the quantum density matrix with different classical trajectories, to avoid the failure caused by the single trajectory description in the mean field method.

For this purpose, we define

$$\Delta Q = \sum_{i\neq j} |\tilde{\mathbf{Q}}_i - \tilde{\mathbf{Q}}_j| \tag{21}$$

where $\tilde{\mathbf{Q}}_i$ denotes the corrected position on the ith potential energy surface, and is calculated from the diagonal terms of $\mathbf{X}$ as $\tilde{\mathbf{Q}}_i = \bar{\mathbf{Q}} + \mathbf{X}_{ii}/\rho_{ii}$. If ΔQ is larger than a certain threshold δ, we branch the mean field trajectory into multiple ones by dividing elements of the density matrix into multiple trajectories (see below for details). The coordinate deviation defined in eq 21 is used as the branching criterion for the following reasons: First, the coordinates determine the forces on the classical DOFs, which is a direct measure of the difference between the potential energy surfaces. Second, deviations of coordinates and momenta are correlated, which means that the momenta deviation will not be neglected although the deviation of coordinates is used as the branching criterion. Of course, it is also possible to use the momenta deviation, or combinations of coordinates and momenta deviations as the branching criterion.

This branching method has utilized the linearity of the MQCL equation, where propagation of the whole phase space density distribution $\rho(\mathbf{Q},\mathbf{P})$ can be divided into propagation of each terms $\rho_{ij}(\mathbf{Q},\mathbf{P})$ and then sum them up. For the branches originated from the diagonal terms of the density matrix (population-like terms), the mean field force is calculated using eq 15 as in the standard mean field method. For the branches originated from the off-diagonal elements of the density matrix (coherence-like terms), we use the average force determined as

$$\mathbf{F} = \frac{1}{2}\mathbf{F}_i + \frac{1}{2}\mathbf{F}_j \tag{22}$$

where i and j are the subscripts of the nonzero density matrix element in the initial branch; i.e., we keep track of the origins of the coherence-like trajectory branches and use them to determine which average force to use.

We note that eq 22 for off-diagonal initial state is more consistent with the force from the MQCL equation. For the diagonal initial state $\rho_{ii} = 1$, the mean field force $\mathbf{F}_{ii}$ is the same as that from the MQCL equation. However, for the off-diagonal initial state $\rho_{ij} = 1$, $i \neq j$, the mean field force $\mathbf{F}_{ij}$ is rather different from the force $(\mathbf{F}_{ii} + \mathbf{F}_{jj})/2$ using the MQCL equation. This can be traced back to eqs 10 and 11, where the diagonal terms of the density matrix are used to define the reference trajectory. Thus, we use eq 22 rather than the mean field force for trajectory branches starting with an off-diagonal initial state.

Details of the trajectory branching method used in this work are summarized as follows:

(1) As in the traditional mean field approximation, initialize the quantum density matrix, as well as the classical positions and momenta at $t = 0$. For each specific initial set of positions and momenta, the number of trajectory branches is 1, which carries the weight $w_1 = 1.0$.

(2) Propagate each trajectory branch from t to $t + \mathrm{d}t$ under the mean field approximation. If the trace of the density matrix is one (i.e., the initial density matrix is population-like), the mean field force in eq 15 is used. If the trace of the density matrix is zero (i.e., the initial density matrix is coherence-like), the force from the average potential in eq 22 is used, where i and j are the subscripts of the nonzero density matrix element that initializes the branch. At the same time, propagate the auxiliary variables $\mathbf{X}$ and $\mathbf{\Pi}$ using eqs 19 and 20.

(3) Decide whether a branching action will take place. If the trajectory displacement defined in eq 21 is smaller than the threshold δ, the mean field dynamics will continue to the next time step by returning to step (2). If $\Delta Q > \delta$, the trajectory will bifurcate into N diagonal and $N(N-1)/2$ off-diagonal branches (assuming N is the total number of electronic states) using the following protocol: (a) For the ith diagonal terms in the density matrix (population-like branches), add a trajectory branch with $\bar{\rho}_{ii} = 1.0$ and set all other terms in the density matrix to zero; set the positions and momenta of the new trajectory branches to $\bar{\mathbf{Q}}_i = \bar{\mathbf{Q}} + \mathbf{X}_{ii}/\bar{\rho}_{ii}$ and $\bar{\mathbf{P}}_i = \bar{\mathbf{P}} + \mathbf{\Pi}_{ii}/\bar{\rho}_{ii}$; the weight of the new trajectory branch is set

dx.doi.org/10.1021/jp503522g | J. Phys. Chem. A XXXX, XXX, XXX−XXX

to $w = w^{old}*\bar{\rho}_{ii}$. (b) For the off-diagonal terms ρ_{ij} with $i \neq j$ (coherence-like branches), set $\bar{\rho}_{ij} = \bar{\rho}_{ij}^{old}/|\bar{\rho}_{ij}^{old}|$, $\bar{\rho}_{ij} = \bar{\rho}_{ji}^{old}/|\bar{\rho}_{ji}^{old}|$, and all other terms in the density matrix to zero; keep the current positions and momenta $\bar{\mathbf{P}}_{ij} = \bar{\mathbf{P}}^{old}$, $\bar{\mathbf{Q}}_{ij} = \bar{\mathbf{Q}}^{old}$; the weight of the new trajectory branch is set to $w = w^{old}*|\bar{\rho}_{ij}^{old}|$.

(4) Return to step (2), and continue until the equations of motion are propagate to a certain number of time steps.

It is clear that the choice of the threshold δ affects the convergence of the trajectory branching method. If δ is too large, the dynamics reduces to the traditional mean field approximation, which were known to have many problems. On the other hand, when δ is too small, the trajectory may branch every time step, and the current method will reduce to a brute force solution to the MQCL equation. But at the same time, the huge number of trajectory branches will limit the method only to short times. So selection of δ should be based on the balance of accuracy and efficiency.

In realistic calculations, the number of trajectory branches may vary for specific problems. If the number of total trajectory branches is not large, one can keep track all of them in the calculation, as in the numerical algorithm presented above. There is another possibility that the systems stay for a long time in the interaction region, which may lead to a large numbers of trajectory branches. In that case, it is possible to use a Monte Carlo sampling scheme to select which trajectory branches to follow, as has been done in the conventional method to simulate the MQCL equation.[50−54] We may also introduce a filtering cutoff δw to discard trajectories that have a very small weight with $|w| < \delta w$. The later method is used in this study if the number of trajectory branches is large.

3. RESULTS

In this section, the new trajectory branching method is applied to several one-dimensional two electronic state models, which have been investigated previously[17,42] to test the SH algorithms in different cases. The results from the new method are compared with those from the mean field and the quantum mechanics methods. We will focus on the improvement of the new method over the traditional mean field approximation, which is found to be inaccurate or totally fail in some parameter regimes.[42,70]

The atomic unit (au) is used in all the calculations. The atomic mass is set to 2000, which is similar to the mass of a hydrogen atom. The benchmark quantum mechanic results are obtained from refs 42 and 43. As found later, in most of the model problems except that in section 3.5, one single initial trajectory is enough to get good results using the trajectory branching method. So in these simulations, the particle starts at position $x = -20$ with a predefined momentum k. In the problem presented in section 3.5, the average over the initial wave packet is needed, and the initial position and momentum are sampled from the Wigner distribution[63] of an initial Gaussian wave packet centered at $x = -20$. The time step in all simulations is set to $dt = 0.3$. The simulations give the transmission and reflection population on the upper and lower states when the trajectories leave the interaction region, where propagation of the trajectories is stopped when x is larger than 25 or smaller than −25. Occasionally, a small number of trajectories are trapped at the interaction region, and trajectories with time steps larger than 500 000 are ignored.

3.1. Extended Coupling with Reflection.

The first example is Tully's problem C in ref 17. We use it as an example to show the advantage of the trajectory branching method over the traditional mean field method when there is significant difference between the two potential energy surfaces. In this model, the diabatic energies and the coupling term are defined as follows:

$$V_{11}(x) = A \tag{23a}$$

$$V_{22}(x) = -A \tag{23b}$$

$$V_{12}(x) = V_{21}(x) = \begin{cases} Be^{Cx} & x \leq 0 \\ B(2 - e^{-Cx}) & x \geq 0 \end{cases} \tag{23c}$$

where $A = 6 \times 10^{-4}$, $B = 0.1$, and $C = 0.9$. The adiabatic potential energy curves and the nonadiabatic coupling term $d_{12}(x)$ are shown in Figure 1a.

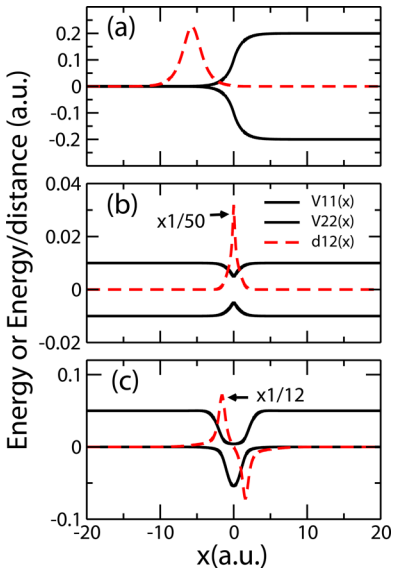

Figure 1. Adiabatic potential energy surfaces (solid lines) and coupling terms (dashed lines) for the model problems in sections 3.1−3.3, which are taken from ref 17. (a) Extended coupling with reflection model. (b) Simple avoided crossing model. (c) Dual avoided crossing model.

The calculated transmission and reflection populations are shown in Figure 2a−c. As stated previously, the quantum results are taken from ref 42, where the initial Gaussian wave packet has a width of 2.0. The threshold δ in the branching criterion is set as 4.0.

When the momentum k is large enough (>30), the quantum wave packet can pass through the whole interaction region without reflection. In such cases, the final populations on the upper and lower states are determined by the short time dynamics in the coupling region, where the mean field approximation may provide a good description. Indeed, both the mean field and trajectory branching methods give the correct result.

However, for smaller k values, motion on the upper state does not have large enough momentum to go over the slope region, and reflection occurs. In this case, the mean field method, which uses a single trajectory to describe the dynamics, is not able to give correct results, as it gives zero reflection

dx.doi.org/10.1021/jp503522g | J. Phys. Chem. A XXXX, XXX, XXX−XXX

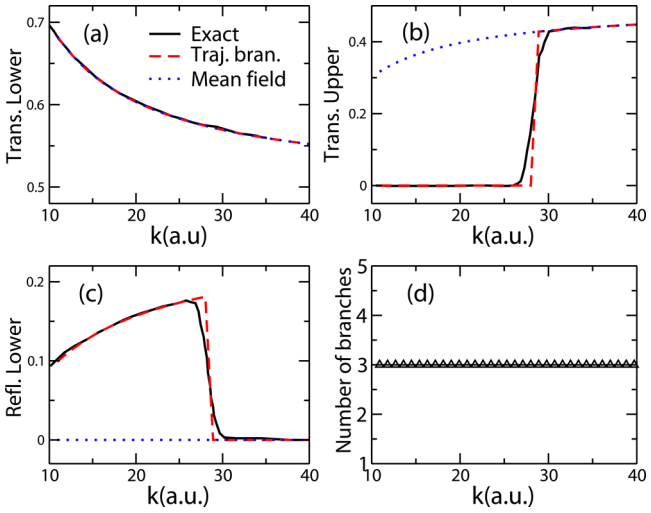

Figure 2. (a)−(c) Transmission and reflection populations on the lower and upper states for the extended coupling with reflection model in section 3.1. The results are calculated from the trajectory branching (dashed line), mean field (dotted line), and exact quantum mechanics (solid line) methods. The exact results are taken from ref 42. (d) Number of the final trajectory branches for each initial momentum.

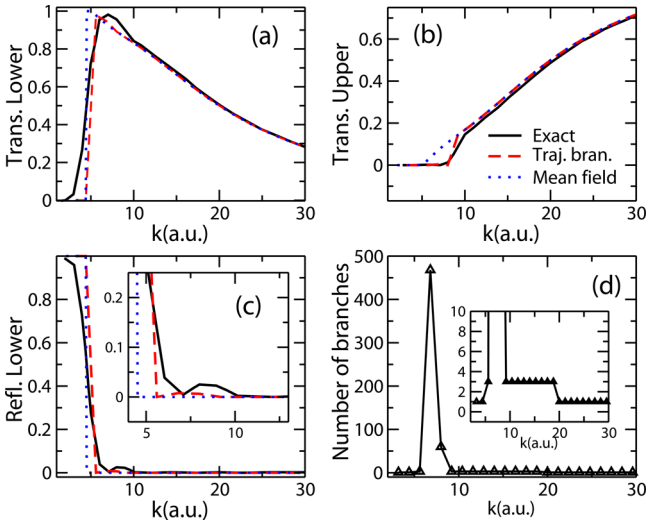

Figure 3. Same as Figure 2, for the simple avoided crossing model in section 3.2. The exact quantum results are taken from ref 43.

population. On the other hand, the trajectory branching method with even a single initial trajectory gives quite good results, which are almost identical to the exact ones, except when k is close to 30, where the turnings of the transmission and reflection curves are too sharp in comparison with the exact quantum results. We note if we sample the initial positions and momenta from the Wigner distribution of the initial Gaussian wave packet, the exact results can be reproduced more accurately. (curves not shown in Figure 2).

Figure 2d shows the number of trajectories in the final state of the trajectory branching method. We can see that for all k values, only one trajectory branching event occurs during the time evolution. In other words, only three trajectories are needed for each k. So for this specific problem, the new method provides a very efficient way to correct the problem of the traditional mean field approach, with just a few times more computational cost.

3.2. Simple Avoided Crossing. This example is Tully's problem A in ref 17. The diabatic potential energies and the coupling term in this model are given by

$$V_{11}(x) = \begin{cases} A(1 - e^{-Bx}) & x \geq 0 \\ -A(1 - e^{Bx}) & x < 0 \end{cases} \quad (24a)$$

$$V_{22}(x) = -V_{11} \quad (24b)$$

$$V_{12}(x) = V_{21}(x) = Ce^{-Dx^2} \quad (24c)$$

where the parameters are set as $A = 0.01$, $B = 1.6$, $C = 0.005$, and $D = 1.0$. The adiabatic potential energy curves and the nonadiabatic coupling term $d_{12}(x)$ are shown in Figure 1b.

Similar to the previous example in section 3.1, when k is larger than 8.9, the reflecting populations on both the lower and upper states tend to zero, and the mean field method gives nearly exact result, as shown in Figure 3a−c. When k is smaller, the mean field method gives zero reflection population on the lower state, while the quantum reflecting population on the lower state is still slightly larger than zero. The trajectory branching method is shown to perform sightly better than the mean field approach in both the transmission and reflection populations, as shown in Figure 3.

The number of final trajectory branches is also shown in Figure 3d, where the branching threshold is set to $\delta = 4.0$. It can be seen that, when k is greater than 20, no branching actions take place, and the new method reduces to traditional mean field method. When $10 < k < 20$, only one trajectory branch occurs. When k is between 3.0 and 10, there is a much larger number of trajectory branches, and filtering of the branches with a weight cutoff of $\delta w = 0.001$ is used. It can be seen that the new method gives better results than the traditional mean field approach in this region.

3.3. Dual Avoided Crossing. This example is Tully's problem B in ref 17, where the diabatic potential energies and the coupling term are given by

$$V_{11}(x) = 0 \quad (25a)$$

$$V_{22}(x) = -Ae^{-Bx^2} + E \quad (25b)$$

$$V_{12}(x) = V_{21}(x) = Ce^{-Dx^2} \quad (25c)$$

Here the parameters are set as $A = 0.1$, $B = 0.28$, $C = 0.015$, $D = 0.06$, and $E = 0.05$. The adiabatic potential energies and the nonadiabatic coupling term are shown in Figure 1c. This model has some similarities with the above one in section 3.2, but the coupling region is separated into two parts.

The results in Figure 4a−c show the comparison of results from different methods. The branching threshold is set to $\delta = 1.0$ in this model. It can be seen that, when k is larger than 30.0, only a small number of trajectory branches are needed, and both the new method and the traditional mean field method give good results. When k is between 20.0 and 30.0, the trajectory branching method also gives similar results to the mean field method, whereas their deviation from the quantum results are likely due to the quantum effect of the nuclear dynamics.

Because of the shape of the upper potential energy curve, when k is smaller, the particle may stay in the valley region and keep moving forward and backward for a long time. This is a more challenging region for the trajectory branching method.

dx.doi.org/10.1021/jp503522g | J. Phys. Chem. A XXXX, XXX, XXX−XXX

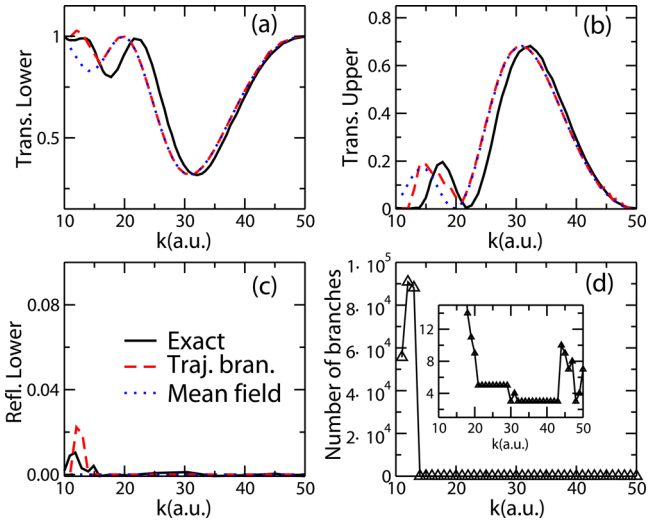

Figure 4. Same as Figure 2, for the dual avoided crossing model in section 3.3.

As shown in Figure 4d, when k is smaller than 15.0, the frequent branching actions lead to a very large number of trajectories, and the trajectory branching method becomes inaccurate.

3.4. Dumbbell Geometry. This example is the Dumbbell model used by Subotnik's in ref 42. It is a symmetrized version of the extended coupling model in section 3.1 The diabatic potential energies and coupling of this model are defined as

$$V_{11}(x) = A \tag{26a}$$

$$V_{22}(x) = -A \tag{26b}$$

$$V_{12}(x) = V_{21}(x) = \begin{cases} Be^{C(x-Z)} + B(2 - e^{C(x+Z)}) & x \le -Z \\ Be^{C(x-Z)} + Be^{-C(x+Z)} & -Z \le x \le Z \\ B(2 - e^{-C(x-Z)}) + Be^{-C(x+Z)} & x \ge Z \end{cases} \tag{26c}$$

where the parameters A, B, C are set as same as ones in section 3.1, and Z = 10. The adiabatic potential energy curves and the nonadiabatic coupling term are shown in Figure 5a. Because the model has two coupling regimes, a more complicated transmission and reflection behavior has been observed, which makes the model a more stringent test of the SH methods.[42,70]

The simulation results are shown in Figure 6a−c, where the branching threshold is set to δ = 4.0. It can be seen that the trajectory branching method can capture almost all the important features of the quantum result. When k > 40, both the new method and the mean field method reproduce the quantum results very well. When k is between 28 and 40, because the particle will move back and forth on the upper potential energy surface, a relatively large number of branching are needed. Nevertheless, by using a filtering cutoff to discard trajectory branches with absolute value of the weights smaller than 0.001, converged results can be obtained with an acceptable number of branches as shown in Figure 6d. In contrast, the mean field method has many problems in this region.

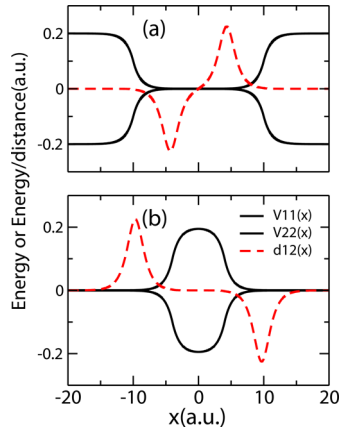

Figure 5. Adiabatic potential energy surfaces (solid lines) and coupling terms (dashed lines) for the model problems in sections 3.4 and 3.5, which are taken from ref 42. (a) Dumbbell model. (b) Double arch model.

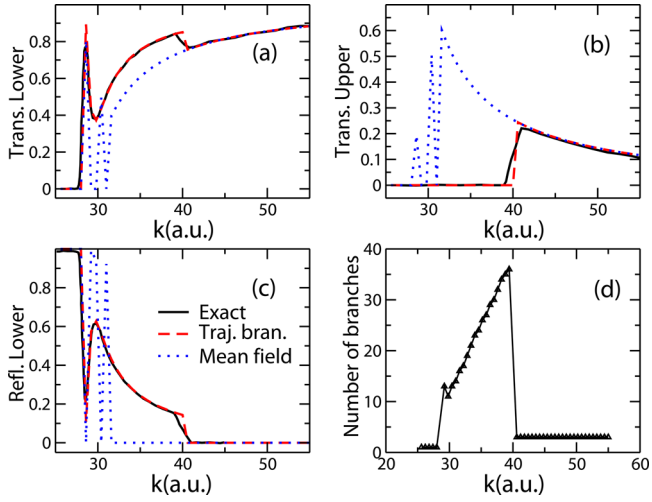

Figure 6. Same as Figure 2, for the dumbbell model in section 3.4.

It has been shown previously, the dumbbell model also causes problems for the FSSH method,[42] so the current results show that the new method can also work with more complex models with limited increase of computational costs.

3.5. Double Arch Model. In the double arch model from ref 42, the diabatic potential energies and coupling term are defined as

$$V_{11}(x) = A \tag{27a}$$

$$V_{22}(x) = -A \tag{27b}$$

$$V_{12}(x) = V_{21}(x) = \begin{cases} -Be^{C(x-Z)} + Be^{C(x+Z)} & x \le -Z \\ -Be^{C(x-Z)} - Be^{-C(x+Z)} + 2B & -Z \le x \le Z \\ Be^{-C(x-Z)} - Be^{-C(x+Z)} & x \ge Z \end{cases} \tag{27c}$$

The parameters A, B, C are set as same as ones in the above model in section 3.1, and Z is set to 4.0. The adiabatic potential energy curves and the nonadiabatic coupling term of this model are shown in Figure 5b, in which the energy curves have the

dx.doi.org/10.1021/jp503522g | J. Phys. Chem. A XXXX, XXX, XXX−XXX

shape of a double arch. In this model, the left half of the potential energy surfaces is similar to the first model in section 3.1, and the right half is the image of the left. It also has two coupling regions, which gives the possibility for quantum interferences between the two surfaces.

The simulation results are given in Figures 7 and 8, where the branching threshold is set to $\delta = 2.0$. When $k < 28$, the particle

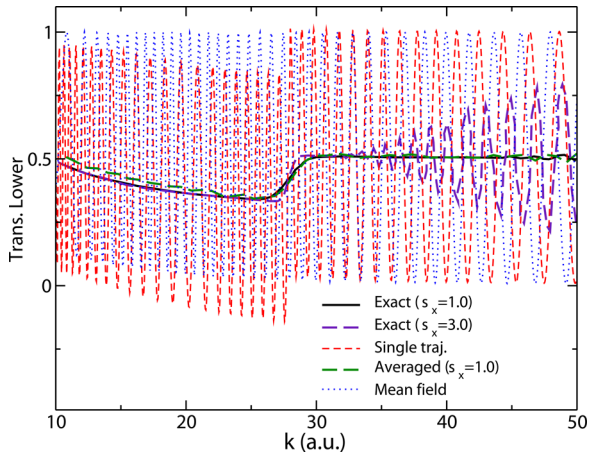

Figure 7. Transmission population on the lower state for the double arch model in section 3.5. The results are calculated from the trajectory branching (dashed line), mean field (dotted line), and exact quantum mechanics (solid line) methods. The exact results are taken from ref 42.

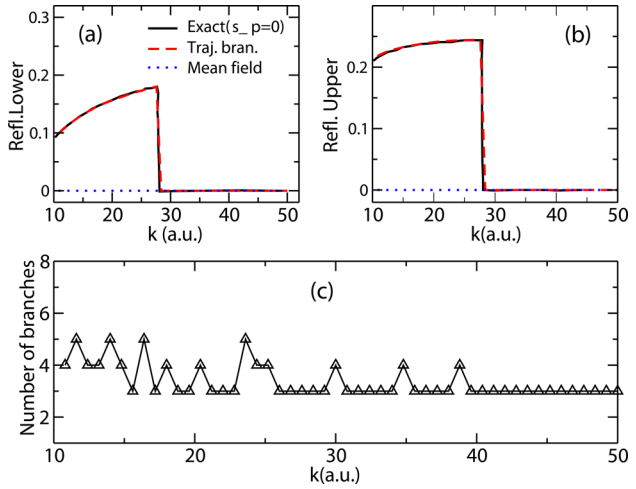

Figure 8. (a, b) Same as Figure 7 for the reflection population on the lower and upper states. (c) Number of the final trajectory branches for each initial momentum, starting from a single trajectory branch at $x = -20$.

in the upper state will reflect and give a reflecting population similar to that in the previous model in section 3.1. Because there is an additional coupling region on the right, different transition populations are obtained in comparing to the results in section 3.1. When k is larger, transmission on both the upper and lower states interfere, leading to oscillations of the transition populations in the lower and upper states, which depends on the width of the incoming wave packet and the initial momentum k.

As can be seen in Figure 8a–c, the trajectory branching method gives correct reflection population, and the number of trajectory branches is also small. However, for the transmission populations, using single initial trajectory results in strong oscillations, and the apearance of negative population values for certain initial momentum k. We note the oscillatory behavior also presents in the traditional mean field method, and the FSSH method.[42] Taking averages using 5000 trajectories with initial positions and momenta sampled from the Wigner transform of the initial Gaussian wave packet ($\sigma_x = 1.0$) is shown to correct the problem of the wrong oscillations, as shown in Figure 7. We also note that, when further increasing the wave packet width ($\sigma_x = 3.0$), the trajectory branching method will not produce the correct oscillations as in the quantum result (simulation results not shown).

Comparison with the results in section 3.1 reveals some interesting details of the trajectory branching method. It is shown that the oscillation with a single initial trajectory is due to coherence-like branches that originates from the off-diagonal term of the density matrix. In section 3.1, there are also relatively large off-diagonal terms, but because the trajectory passes the interaction region only once, the off-diagonal terms do not influence the populations. However, in this model, passing through the coupling region again in the right half bring back the effect of the off-diagonal terms, which leads to the oscillation of populations.

4. CONCLUSIONS AND DISCUSSIONS

In this paper, we have proposed a new trajectory branching algorithm to modify the popular mean field method, based on an approximate method to propagate the MQCL equation. A new set of variables are defined to measure the deviation of the trajectories on different potential energy surfaces from the reference mean field trajectory. Dynamics of the new set of variables is derived from the MQCL equation using the method of first moment expansion. And finally, the trajectory branching method is designed utilizing the linearity of the MQCL equation.

Numerical results show that the new method can indeed perform better than the mean field approach by going beyond the single trajectory approximation. Among the examples presented in section 3, problems 3.1 and 3.4 are the most successful, where the new method corrects the problem of traditional mean field approach with only a small number of trajectory branches. Although in the small k region in problem 3.3, there are frequent crossing and recrossing of the interaction region, the large number of trajectory branches leads to the failure of the new method in this regime.

Because the new method is based on the mean field method, it has some inherent features of the mean field approach. The good thing is that the mean field dynamics is reasonably robust, and the method will also share some deficiencies of the traditional mean field method, such as lack of nuclear quantum effects, and the unphysical oscillations in Problem 3.5. The new method seems to work better in cases where the adiabatic potential energy surfaces are significant different, and in cases where there are not many recrossings of the interaction region.

In summary, using the new trajectory branching method, we have shown some encouraging examples where the single trajectory approximation can be corrected in a relatively simple way. In future studies, it would be possible to incorporate other ideas of trajectory branching[44,46] to further improve the current method. We note that the model problems used in this study are all based on the scattering problem, further tests of the new

dx.doi.org/10.1021/jp503522g | J. Phys. Chem. A XXXX, XXX, XXX–XXX

method in condensed phase problems would also be interesting.

AUTHOR INFORMATION

Corresponding Author

*Q. Shi. E-mail: qshi@iccas.ac.cn. Phone: +86-10-82616163. Fax: +86-10-82616163.

Notes

The authors declare no competing financial interest.

ACKNOWLEDGMENTS

This work is supported by NSFC (Grant Nos. 91027015, 21290194), the 973 program (Grant Nos. 2011CB808502, 2013CB933501), and the Strategic Priority Research Program of the Chinese Academy of Sciences (Grant No. XDB12020300).

REFERENCES

(1) Berne, B. J., Ciccotti, G., Coker, D. F., Eds. *Classical and Quantum Dynamics in Condesed Phase Simulations*; World Scientific: NJ, 1998.

(2) Beck, M. H.; Jčkle, A.; Worth, G. A.; Meyer, H. D. The Multiconfiguration Time-dependent Hartree (MCTDH) Method: A Highly Efficient Algorithm for Propagating Wavepackets. *Phys. Rep.* **2000**, *324*, 1−105.

(3) Meyer, H. D.; Worth, G. A. Quantum Molecular dynamics: Propagating Wavepackets and Density Operators Using the Multi-configuration Time-dependent Hartree (MCTDH) Method. *Theor. Chem. Acc.* **2003**, *109*, 251−267.

(4) Wang, H.; Thoss, M. Multilayer Formulation of the Multi-configuration Time-dependent Hartree Theory. *J. Chem. Phys.* **2003**, *119*, 1289−1299.

(5) Makri, N.; Makarov, D. Tensor Propagator for Iterative Quantum Time Evolution of Reduced Density-Matrices 0.1. Theory. *J. Chem. Phys.* **1995**, *102*, 4600−4610.

(6) Mak, C.; Egger, R. Monte Carlo Methods for Real-time Path Integration. *Adv. Chem. Phys.* **1996**, *93*, 39−76.

(7) Tanimura, Y. Stochastic Liouville, Langevin, Fokker-Planck, and Master Equation Approaches to Quantum Dissipative Systems. *J. Phys. Soc. Jpn.* **2006**, *75*, 082001−082039.

(8) Jin, J. S.; Zheng, X.; Yan, Y. J. Exact Dynamics of Dissipative Electronic Systems and Quantum Transport: Hierarchical Equations of Motion Approach. *J. Chem. Phys.* **2008**, *128*, 234703−234717.

(9) Shi, Q.; Chen, L. P.; Nan, G. J.; Xu, R. X.; Yan, Y. J. Efficient Hierarchical Liouville-Space Propagator to Quantum Dissipative Dynamics. *J. Chem. Phys.* **2009**, *130*, 084105−084108.

(10) Heller, E. J. Cellular Dynamics: A New Semiclassical Approach to Time-Dependent Quantum Mechanics. *J. Chem. Phys.* **1991**, *94*, 2723−2729.

(11) Stock, G.; Thoss, M. Semiclassical Description of Nonadiabatic Quantum Dynamics. *Phys. Rev. Lett.* **1997**, *78*, 578−581.

(12) Miller, W. H. The Semiclassical Initial Value Representation: A Potentially Practical Way for Adding Quantum Effects to Classical Molecular Dynamics Simulations. *J. Phys. Chem. A* **2001**, *105*, 2942−2955.

(13) Shi, Q.; Geva, E. Semiclassical Theory of Vibrational Energy Relaxation in the Condensed Phase. *J. Phys. Chem. A* **2003**, *107*, 9059−9069.

(14) Thoss, M.; Wang, H. B. Semiclassical Description of Molecular Dynamics Based on Initial-value Representation Methods. *Annu. Rev. Phys. Chem.* **2004**, *55*, 299−332.

(15) Meyer, H. D.; Miller, W. H. Classical Analog for Electronic Degrees of Freedom in Non-Adiabatic Collision Processes. *J. Chem. Phys.* **1979**, *70*, 3214−3223.

(16) Billing, G. D. Quantum Corrections to the Classical Path Theory. *J. Chem. Phys.* **1993**, *99*, 5849−5857.

(17) Tully, J. C. Molecular Dynamics with Electronic Transitions. *J. Chem. Phys.* **1990**, *93*, 1061−1071.

(18) Webster, F. J.; Rossky, P. J.; Friesner, R. A. Nonadiabatic Processes in Condensed Matter: Semiclassical Theory and Implementation. *Comput. Phys. Commun.* **1991**, *63*, 494−522.

(19) Kapral, R.; Ciccotti, G. Mixed Quantum-Classical Dynamics. *J. Chem. Phys.* **1999**, *110*, 8919−8929.

(20) Ben-Nun, M.; Martinez, T. J. Ab Initio Quantum Molecular Dynamics. *Adv. Chem. Phys.* **2002**, *121*, 439−512.

(21) Hammes-Schiffer, S.; Tully, J. C. Proton Transfer in Solution: Molecular Dynamics with Quantum Transitions. *J. Chem. Phys.* **1994**, *101*, 4657−4667.

(22) Landry, B. R.; Subotnik, J. E. Communication: Standard Surface Hopping Predicts Incorrect Scaling for Marcus Golden-rule Rate: The Decoherence Problem Cannot be Ignored. *J. Chem. Phys.* **2011**, *135*, 191101−191104.

(23) Xie, W.; Bai, S.; Zhu, L.; Shi, Q. Calculation of Electron Transfer Rates Using Mixed Quantum Classical Approaches: Nonadiabatic Limit and Beyond. *J. Phys. Chem. A* **2013**, *117*, 6196−6204.

(24) Stock, G.; Thoss, M. Classical Description of Nonadiabatic Quantum Dynamics. *Adv. Chem. Phys.* **2005**, *131*, 243−375.

(25) Sulc, M.; Hernandez, H.; Martinez, T. J.; Vanicek, J. Relation of Exact Gaussian Basis Methods to the Dephasing Representation: Theory and Application to Time-resolved Electronic Spectra. *J. Chem. Phys.* **2013**, *139*, 034112−034124.

(26) van der Vegte, C. P.; Dijkstra, A. G.; Knoester, J.; Jansen, T. L. C. Calculating Two-Dimensional Spectra with the Mixed Quantum-Classical Ehrenfest Method. *J. Chem. Phys. A* **2013**, *117*, 5970−5980.

(27) Jose Bajo, J.; Gonzalez-Vazquez, J.; Sola, I. R.; Santamaria, J.; Richter, M.; Marquetand, P.; Gonzalez, L. Mixed Quantum-Classical Dynamics in the Adiabatic Representation To Simulate Molecules Driven by Strong Laser Pulses. *J. Phys. Chem. A* **2012**, *116*, 2800−2807.

(28) Yonehara, T.; Hanasaki, K.; Takatsuka, K. Fundamental Approaches to Nonadiabaticity: Toward a Chemical Theory Beyond the Born-Oppenheimer Paradigm. *Chem. Rev.* **2012**, *112*, 499−542.

(29) Born, M.; Oppenheimer, R. Quantum Theory of Molecules. *Annalen Der Physik* **1927**, *84*, 0457−0484.

(30) Gerber, R. B.; Buch, V.; Ratner, M. A. Time-Dependent Self-Consistent Field Approximation for Intramolecular Energy-Transfer 0.1. Formulation and Application to Dissociation of Vanderwaals Molecules. *J. Chem. Phys.* **1982**, *77*, 3022−3030.

(31) Stock, G. A Semiclassical Self-Consistent-Field Approach to Dissipative Dynamics - the Spin-Boson Problem. *J. Chem. Phys.* **1995**, *103*, 1561−1573.

(32) Tully, J. C.; Preston, R. K. Trajectory Surface Hopping Approach to Nonadiabatic Molecular Collisions: Reaction of H+ with D2. *J. Chem. Phys.* **1971**, *55*, 562−572.

(33) Coker, D. F.; Xiao, L. Methods for Molecular-Dynamics with Nonadiabatic Transitions. *J. Chem. Phys.* **1995**, *102*, 496−510.

(34) Hammes-Schiffer, S. Mixed Quantum/Classical Dynamics of Hydrogen Transfer Reactions. *J. Phys. Chem. A* **1998**, *102*, 10443−10454.

(35) Parandekar, P. V.; Tully, J. C. Detailed Balance in Ehrenfest Mixed Quantum-Classical Dynamics. *J. Chem. Theory Comput.* **2006**, *2*, 229−235.

(36) Bastida, A.; Cruz, C.; Zuniga, J.; Requena, A.; Miguel, B. The Ehrenfest Method with Quantum Corrections to Simulate the Relaxation of Molecules in Solution: Equilibrium and Dynamics. *J. Chem. Phys.* **2007**, *126*, 014503−014513.

(37) Tully, J. C. Perspective: Nonadiabatic Dynamics Theory. *J. Chem. Phys.* **2012**, *137*, 22A301−22A307.

(38) Tully, J. C. Mixed Quantum-Classical Dynamics. *Faraday Discuss.* **1998**, *110*, 407−419.

(39) Bittner, E. R.; Rossky, P. J. Quantum Decoherence in Mixed Quantum-Classical Systems: Nonadiabatic Processes. *J. Chem. Phys.* **1995**, *103*, 8130−8143.

(40) Hack, M. D.; Truhlar, D. G. A Natural Decay of Mixing Algorithm for Non-Born-Oppenheimer Trajectories. *J. Chem. Phys.* **2001**, *114*, 9305−9314.

(41) Zhu, C.; Jasper, A. W.; Truhlar, D. G. Non-Born-Oppenheimer Trajectories with Self-consistent Decay of Mixing. *J. Chem. Phys.* **2004**, *120*, 5543−5557.
(42) Subotnik, J. E.; Shenvi, N. A New Approach to Decoherence and Momentum Rescaling in the Surface Hopping Algorithm. *J. Chem. Phys.* **2011**, *134*, 024105−024123.
(43) Subotnik, J. E. Augmented Ehrenfest Dynamics Yields a Rate for Surface Hopping. *J. Chem. Phys.* **2010**, *132*, 134112−134130.
(44) Yonehara, T.; Takatsuka, K. Phase-Space Averaging and Natural Branching of Nuclear Paths for Nonadiabatic Electron Wavepacket Dynamics. *J. Chem. Phys.* **2008**, *129*, 134109−134121.
(45) Belyaev, A. K.; Lebedev, O. V. Nonadiabatic Nuclear Dynamics of Atomic Collisions Based on Branching Classical Trajectories. *Phys. Rev. A* **2011**, *84*, 014701−014704.
(46) Yonehara, T.; Takatsuka, K. Path-Branching Representation for Nonadiabatic Electron Dynamics in Conical Intersection. *J. Phys. Chem. A* **2013**, *117*, 8599−8608.
(47) Gerasimenko, V. I. Dynamical Equations of Quantum-Classical: Systems. *Theor. Math. Phys.* **1982**, *50*, 49−55.
(48) Kapral, R. Quantum-Classical Dynamics in a Classical Bath. *J. Phys. Chem. A* **2001**, *105*, 2885−2889.
(49) Ando, K.; Santer, M. Mixed Quantum-Classical Liouville Molecular Dynamics without Momentum Jump. *J. Chem. Phys.* **2003**, *118*, 10399−10406.
(50) Shi, Q.; Geva, E. A Derivation of the Mixed Quantum-Classical Liouville Equation from the Influence Functional Formalism. *J. Chem. Phys.* **2004**, *121*, 3393−3404.
(51) Horenko, I.; Salzmann, C.; Schmidt, B.; Schutte, C. Quantum-Classical Liouville Approach to Molecular Dynamics: Surface Hopping Gaussian Phase-Space Packets. *J. Chem. Phys.* **2002**, *117*, 11075−11088.
(52) Santer, M.; Manthe, U.; Stock, G. Quantum-classical Liouville Description of Multidimensional Nonadiabatic Molecular Dynamics. *J. Chem. Phys.* **2001**, *114*, 2001−2012.
(53) Mac Kernan, D.; Ciccotti, G.; Kapral, R. Surface-Hopping Dynamics of a Spin-Boson System. *J. Chem. Phys.* **2002**, *116*, 2346−2353.
(54) Kapral, R. Progress in The Theory of Mixed Quantum-Classical Dynamics. *Annu. Rev. Phys. Chem.* **2006**, *57*, 129−157.
(55) Huo, P.; Coker, D. F. Communication: Partial Linearized Density Matrix Dynamics for Dissipative, Non-Adiabatic Quantum Evolution. *J. Chem. Phys.* **2011**, *135*, 201101−201104.
(56) Huo, P.; Miller, T. F.; Coker, D. F. Communication: Predictive Partial Linearized Path Integral Simulation of Condensed Phase Electron Transfer Dynamics. *J. Chem. Phys.* **2013**, *139*, 151103−151106.
(57) Hsieh, C.-Y.; Kapral, R. Analysis of the Forward-Backward Trajectory Solution for the Mixed Quantum-Classical Liouville Equation. *J. Chem. Phys.* **2013**, *138*, 134110−134121.
(58) Hsieh, C.-Y.; Kapral, R. Nonadiabatic Dynamics in Open Quantum-Classical Systems: Forward-Backward Trajectory Solution. *J. Chem. Phys.* **2012**, *137*, 22a507−22a517.
(59) Kim, H.; Kapral, R. Nonadiabatic Quantum-Classical Reaction Rates with Quantum Equilibrium Structure. *J. Chem. Phys.* **2005**, *123*, 194108−194117.
(60) Rank, J. P.; Kapral, R. Decoherence and Quantum-Classical Dynamics in a Dissipative Bath. *J. Chem. Phys.* **2010**, *132*, 074106−074112.
(61) Subotnik, J. E.; Ouyang, W.; Landry, B. R. Can We Derive Tully's Surface-Hopping Algorithm from the Semiclassical Quantum Liouville Equation? Almost, but only with Decoherence. *J. Chem. Phys.* **2013**, *139*, 214107−214122.
(62) Bai, S.; Xie, W.; Zhu, L.; Shi, Q. Calculation of Absorption Spectra Involving Multiple Excited States: Approximate Methods Based on the Mixed Quantum Classical Liouville Equation. *J. Chem. Phys.* **2014**, *140*, 084105−084114.
(63) Wigner, E. On the Quantum Correction for Thermodynamic Equilibrium. *Phys. Rev.* **1932**, *40*, 0749−0759.
(64) Shi, Q.; Geva, E. A Semiclassical Generalized Quantum Master Equation for an Arbitrary System-Bath Coupling. *J. Chem. Phys.* **2004**, *120*, 10647−10658.
(65) Ryabinkin, I. G.; Hsieh, C.-Y.; Kapral, R.; Izmaylov, A. F. Analysis of Geometric Phase Effects in the Quantum-Classical Liouville Formalism. *J. Chem. Phys.* **2014**, *140*, 084104−084110.
(66) Kernan, D. M.; Ciccotti, G.; Kapral, R. Trotter-Based Simulation of Quantum-Classical Dynamics. *J. Phys. Chem. B* **2008**, *112*, 424−432.
(67) Horsfield, A. P.; Bowler, D. R.; Fisher, A. J.; Todorov, T. N.; Sánchez, C. G. Correlated Electron-Ion Dynamics: the Excitation of Atomic Motion by Energetic Electrons. *J. Phys. Cond. Matter* **2005**, *17*, 4793−4812.
(68) McEniry, E. J.; Bowler, D. R.; Dundas, D.; Horsfield, A. P.; Sánchez, C. G.; Todorov, T. N. Dynamical Simulation of Inelastic Quantum Transport. *J. Phys. Cond. Matter* **2007**, *19*, 196201−196223.
(69) Stella, L.; Meister, M.; Fisher, A. J.; Horsfield, A. P. Robust Nonadiabatic Molecular Dynamics For Metals and Insulators. *J. Chem. Phys.* **2007**, *127*, 214104−214118.
(70) Shenvi, N.; Subotnik, J. E.; Yang, W. T. Simultaneous-Trajectory Surface hopping: A Parameter-Free Algorithm for Implementing Decoherence in Nonadiabatic Dynamics. *J. Chem. Phys.* **2011**, *134*, 144102−144113.